Since January 2020 Elsevier has created a COVID-19 resource centre with free information in English and Mandarin on the novel coronavirus COVID-19. The COVID-19 resource centre is hosted on Elsevier Connect, the company's public news and information website.

Journal of Saudi Chemical Society (2021) **25**, 101348

King Saud University

Journal of Saudi Chemical Society

www.ksu.edu.sa
www.sciencedirect.com

ORIGINAL ARTICLE

Optimization and predictive modelling for the diameter of nylon-6,6 nanofibers via electrospinning for coronavirus face masks

Malihe Zeraati [a], **Rana Pourmohamad** [b], **Bahareh Baghchi** [c], **Narendra Pal Singh Chauhan** [d,*], **Ghasem Sargazi** [e,*]

[a] *Department of Materials Engineering, Shahid Bahonar University of Kerman, 761694111 Kerman, Iran*
[b] *ASU School of Computing, Informatics, and Decision System Engineering, Arizona State University, Tempe, AZ 85281, USA*
[c] *Department of Emergency Medicine, School of Medicine Science, Kermanshah, Iran*
[d] *Department of Chemistry, Faculty of Science, Bhupal Nobles' University, Udaipur 313002, Rajasthan, India*
[e] *Noncommunicable Diseases Research Center, Bam University of Medical Sciences, Bam, Iran*

Received 7 July 2021; revised 11 August 2021; accepted 5 September 2021
Available online 11 September 2021

KEYWORD

Nylon;
Nanofiber;
Electrospinning;
Coronavirus;
Gene expression programming;
Genetic;
Algorithms

Abstract Currently, the only widely available tool for controlling the SARS-CoV-2 pandemic is nonpharmacological interventions (NPIs). Coronavirus aerosols are around 0.3–2 μm in diameter (0.9 m in mass). The present study used artificial intelligence such as gene expression programming (GEP) and genetic algorithms (GA) were used to predict and optimize the diameter of Nylon-6,6 nanofibers via electrospinning for protection against coronavirus. It is suggested that using the controlled experimental conditions such as concentration of nylon-6,6 (16% wt/v), applied voltage (26 kV), working distance (18 cm) and injection rate (0.2 mL/h) have resulted the diameter of nylon-6,6 nanofibers about 55.8 nm. Coronavirus face masks could use the obtained diameter and electrostatic interaction between viral particles and naofibers as active layers.

1. Introduction

In personal protection, facial masking, respirator and ventilator care, an unprecedented concern is being caused by the recent new coronavirus pandemic (COVID-19), for adequate airborne protection [1,2]. More than 2.7 million people in 210 countries around the world were infected with over 180,000 dead in the four months since the outbreak began in mid-December 2019. These staggering statistics are still rising exponentially and far exceed the number the 2003 SARS coro-

* Corresponding authors.
E-mail addresses: narendrapalsingh14@gmail.com, narenpolymer@gmail.com (N.P. Singh Chauhan), g.sargazi@gmail.com (G. Sargazi).
Peer review under responsibility of King Saud University.

ELSEVIER Production and hosting by Elsevier

https://doi.org/10.1016/j.jscs.2021.101348

navirus outbreak, which resulted in 8098 reports of 774 deaths over an eight-month period [3].

Coronavirus is 60–140 nm in size, with nanospikes measuring 9–12 nm in height on its spherical viral capsid/envelope [4]. SARS (Severe acute respiratory syndrome) and MERS (middle East respiratory syndrome) are also a member of the coronavirus family. SARS virus is approximately 81 ± 11 nm in size [5,6] with at least 15 spikes [5]. The spherical form of MERs is 118–136 nm in diameter and has a surface area of 16–21 nm. The spikes of the virus appear as a corona wrapped around the virus, hence the name coronavirus, under the scanning electron microscope [4]. The spikes of the virus (largely protein) serve as anchors to the carrier and host cells of the virus. Some viruses have more spikes than others, such as coronaviruses. The famous Influenza virus, with a majority of 120 nm and a spikes that are not visible, affects a significant number of people and causes many deaths in the flu season [7]. Influenza A, one of the influenzas, is 100 nm in size [8]. All such viruses can be aerosolized as they can be attached by the infected person to fine aerosols (solid particle or droplet), however the coronavirus is better equipped with prominents to anchor its carriers and its host cells during transport. They can be transmitted during flight to environmental aerosols after the air is transmitted. Microbes within droplet nuclei (particles 5 m in diameter) remains in the air for long periods of time and are transmitted greater than 1 m in droplet transmission. Air pollution is similar, since the finer the particles are, the longer they are suspended in the air and the more they can travel. The minimum size of the coronavirus is about 60 nm. Face coverings are thought to reduce aerosol transmission for people standing or sitting next to or behind the coughing or sneezing [9]. According to recent review by Tabatabaeizadeh, there is a link between wearing a face mask and lowering COVID-19 levels [10]. Many physicians have used the elastomeric face mask, which is commonly used in industry, with an extremely low failure rate against coronavirus [11].

Gas masks with asbestos fibre as a filter material first appeared during World War I. The United States developed glass fibre filter materials and issued patents in 1940. Fiber filter materials advanced rapidly from the 1950s to the 1970s, and high-efficiency air filters (HEPA) with glass fibres as filter materials appeared and were used for room air purification [12]. High-efficiency filters made of ultrafine glass fibres with optimized diameter below 0.3 μm are being used to further improve filtration performance, and the filtration efficiency of particles greater than or equal to 0.3 m reaches 99.998%. Following that, Japan developed an ultra-high efficiency filter, with a filtration efficiency of 0.1 m particles reaching as high as 99.9955%. By using an electrostatic mechanism, the ultrathin PMAA (poly(methacrylic acid)) hydrogel obtained can retain its cationic antimicrobial property [13]. With the emergence and development of new industries, such as electronics, aerospace, precision instruments, which require a high degree of indoor air cleanliness, micron level fiber filter materials have failed to meet the requirements of filtration accuracy [14]. It is an inevitable trend for the development of filter materials to use nano-sized fibers in the structure of filter materials. Combining antiviral and filtration properties increases the mask's durability and reliability, reducing the risk of cross-infection [15]. A flexible immunosensor based on a high density conductive nanowire array, a miniaturized impedance circuit, and wireless communication units were embedded in an intelligent face mask developed by Xue and coworkers [16]. In addition, the sub-100 nm size and the gap between neighbouring nanowires make it easier for virus particles to be locked in by the nanowire arrays, improving detection efficiency. There are many methods to prepare nanofiber filter materials, such as drawing, template synthesis, separation of different phases, self-assembly, and electrospinning [17–20]. However, electrospinning is the simplest way to prepare nanofibers [21].

By changing the process parameters during manufacturing, electrospinning is a cost-effective technique for fabricating nanofibers with desired properties. The fiber quality and the diameter are affected by both on solution properties such as viscosity, surface tension and also electrospinning process parameters [22]. Electrospun nanofibers can be used in a variety of applications such as sensors, membranes, wound dressings, drug delivery, and tissue engineering [23–26]. The control of the size and morphology of electrospun nanofibers is an inevitable approach to achieving the desired mechanical, electrical, optical and biomedical properties. Zhang et al. have investigated the effect of solution and process parameters on filtration efficiency in nylon-6,6 [27]. Wu and Dzenis [28] have demonstrated that a changing of the radius of nanofibers could alter the behaviour of true axial nanofibers stress against the axial tensile strain. Due to the nano-effect, He and coworkers [29] have reported that electrospun nanofibers having less than 100 nm in diameters reveal unusual tensile strength, surface reactivity and excellent electrical and thermal conductivity. The one-factor-by-a-time approach to recognising relationships between electrospinning parameters and size/morphology is not only time consuming but probably also inefficient, due to the high level of complexity of the electrospinning process [30,31]. As a result, many studies have examined the effects of process parameters on the size and morphology of the nanofibers produced using statistical techniques [32–36]. With a pressure drop of less than 30 Pa, Leung and Sun have developed a facemask that captures 90% of COVID-19 at 100 nm [37].

Genetic programming (GP), a robust soft computing technique, is advantageous because it develops the model without assuming the prior form of the existing relationship [38]. Gene expression programming (GEP) is an extension of GP, which has the advantage of being able to represent the output with simplified mathematical equations that are suitable for practical application and have a higher prediction accuracy in the fields of materials and biomaterials [39].

The GEP simulation was used for determine the diameter of nanofibers in the previous study [40]. In this paper, we have focused to develop the GEP model for the prediction of electrospun nylon-6,6 fiber diameter as a function of concentration, voltage, distance and rate. Afterward, genetic algorithms (GAs) were used to optimize these electrospinning parameters to have user defined nano fiber diameter. Flowchart of this study is depicted in Fig. 1.

2. Materials and methods

2.1. Experimental

HiTek Power Company (UK) provided a power supply with positive polarity, a voltage range of 1–50 kV, and a maximum amperage of 2 mA and controlling the throughput of the poly-

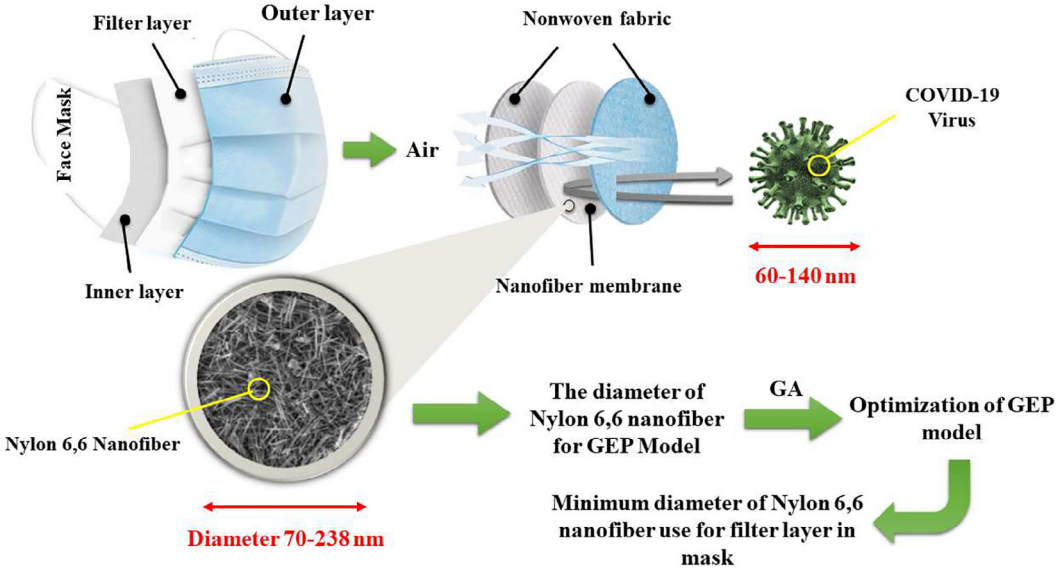

Fig. 1 Flowchart of this study.

mer solution was done with a Stoelting Co. (USA) microsyringe pump. As fibre collectors, aluminium foils (40*60 cm) were used. The polymer solution reservoir and nozzle for electrospinning were used in plastic syringes equipped with metal needles. The polymer solution in the syringe was charged using one electrode from the power supply.

Nylon 6,6 solutions were electrospun from syringes mounted on a syringe pump, which provided different flow rates. Technical grade of nylon 6,6 (M_W = 17000) was dissolved in synthetic grade of formic acid (Merck Chemical Co.) to a concentration of 20–30 w/v %. In all the cases, the nylon 6,6 solution was electrospun from a syringe needle charged to 15–22.5 kV. The distance (d) for electrospinning was 10–20 cm.

2.2. Characterization

The average diameter of the gold-sputtered electrospun nanofibers was determined using scanning electron microscopy (ZEISS DSM 960A, Oberkochen, Germany), and the distribution was obtained by measuring about 100 random nanofibers.

2.3. Data collection

The electrospun has a number of operational parameters that can be adjusted and have an impact on the final results. The operational parameters used are tabulated in Table 1. There are 102 data points taken for present investigation and these data points were used by other researchers [41–45]. A common way to show the distribution and outliers of input data is to use a box plot (Fig. 2) [46].

In order to improve the accuracy and performance of modelling techniques, independent input data is required. A common method for determining the magnitude and direction of practical parameter relationships is bivariate correlation analysis. The accuracy of proposed models was greatly reduced by high negative or positive correlation coefficients between pairs, which enhanced the evolved challenges in understanding the effect of input dimensionless data on the nanofiber diameter of nylon 6,6 as a response [47,48]. The correlation coefficients are shown in Table 2.

If the input data is interactive, the multicollinearity between practical parameters must be determined with the principal component analysis (PCA) of the input parameters. PCA provides the possibility of dimension reduction by transferring from a multi-dimensional space to a lower dimension space. These uncorrelated variables named in new space named principle component [49–51]. The Kaiser Mayer Olkin (KMO) factor [36] should be estimated at the Eq. (1) threshold to ensure PCA possibilities [52].

$$KMO = \frac{\sum\sum r_{ij}^2}{\sum\sum r_{ij}^2 + \sum\sum a_{ij}^2} \quad (1)$$

In which, a_{ij} and r_{ij} are the practical correlation coefficient of i and j variables and the correlation coefficient, respectively. When the KMO factor is less than 0.7, the relationship between the practical parameters is erroneous, and the data is unsuitable for PCA analysis [53]. In this study, the KMO factor is estimated to be 0.568. In the simulation procedure, all 102 data were used and according to Table 4, 71 data were selected as train and 31 data were selected as tests.

Table 1 Experimental ranges.

Concentration (C) (% wt/v)	Voltage (V) kV)	Distance (D) (cm)	Rate (R) (mL/h)	Diameter (nm)
16–25	17–26	8–18	0.2–1.5	70–238

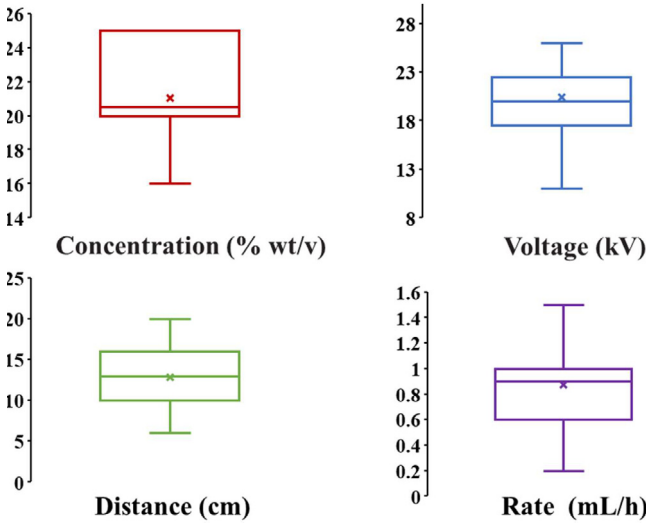

Fig. 2 Boxplot of practical parameters in electrospun nanofiber diameter of Nylon 6,6.

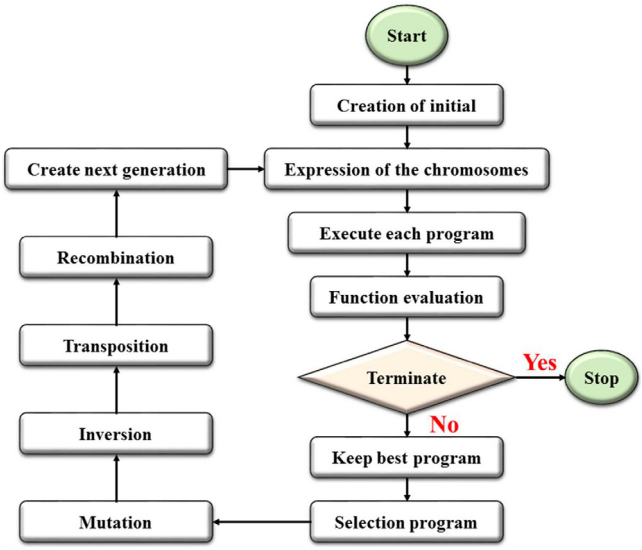

Fig. 3 A typically GEP flowchart.

2.4. Gene expression programming (GEP)

Genetic programming (GP) is an enhanced version of genetic algorithm (GA) that proposed by Koza [54]. To overcome the disadvantageous of GA and GP algorithms, a new populationbased evolutionary algorithm, named gene expression programming (GEP), was introduced by Ferreira [55,56]. Inherent ability of GEP to illustrate an equation by consideration of independent practical parameters as input to estimate the predefined output with acceptance accuracy distinguish GEP respect to the other modeling approaches [57].

The terminal set, termination condition, fitness function, control parameters, and function set are the main components of GEP [54]. Fig. 3 illustrates a typically GEP flowchart. Accordingly, the main portion of GEP is belonging to the genetic operators [58,59]. Since, the operators of genetic operates at level of chromosome, enhanced the simplicity of genetic diversity creation. It was necessary to note that, GEP has a multi-gene nature and consequently each chromosomes including of one or more genes illustrates a mathematical function [58]. There are various methods for the representation of GEP output including Karva language (i.e. is the gene language), expression tree (*ET*) and mathematical function [60,61].

$$(\log(a) + ((2+b) - (c \times a))) \times \left(\sqrt{b/8}\right) \tag{2}$$

The most common methodology for illustrating GEP-generated solution population is the expressive tree (ET). The typical ET for Eq. (2) is illustrated in Fig. 4 [62].

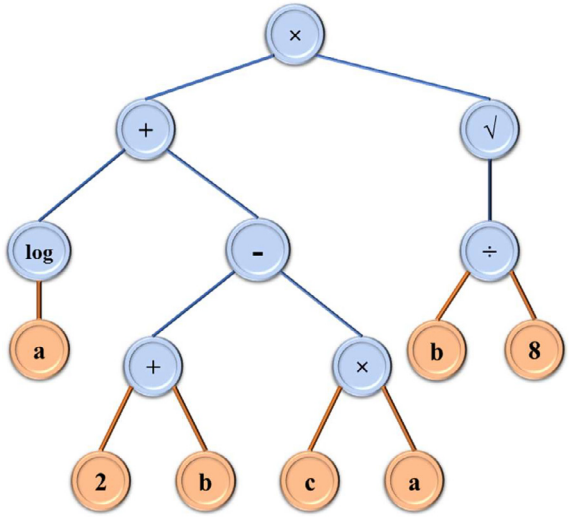

Fig. 4 Typical representation of ET for Eq. (2).

GEP is performed in five major steps:

I. Selection of fitness function (F_i) as Eq. (3) [63]:

$$F_i = \sum_{j=1}^{K_t} \left(R - \left|C_{(i,j)} - T_j\right|\right) \tag{3}$$

Where, R determined as selection range, $C_{(i,j)}$ defined as the value returned by chromosome i by employment of the fitness

Table 2 Correlation coefficients among the electrospun nanofiber diameter of Nylon 6,6.

Parameter	Concentration (% wt/v)	Voltage (kV)	Distance (cm)	Rate (mL/h)
Concentration (% wt/v)	1.000	0.130	0.016	−0.058
Voltage (kV)	0.130	1.000	0.000	0.128
Distance (cm)	0.016	0.000	1.000	−0.127
Rate (mL/h)	−0.058	0.128	−0.127	1.000

function and T_j is defined as the target value corresponding to the fitness function j. If for all j cases, the precision i.e., $|C_{(i,j)} - T_j|$ was less or equal to 0.01, then $F_i = F_{max} = K_t \times M$. In this study, M supposed to 100 and consequently $F_{max} = 1000$. In this way, the system capable to find the optimal solution for itself [28–29].

II. Selection of
   a. terminals (S);
   b. set of functions (F) to generate the chromosomes, as "F" = (Concentration (C), Voltage (V), Distance (D) *and* Rate (R));
   c. arithmetic operators ($+$, $-$, *, /) and
   d. mathematical functions as Exp, Log, Ln, Abs, X [2], X [3], X [4], Sin, Cos and etc. Table 3 typically abbreviates some of trials for GEP modeling.

III. Selection of the chromosomal architecture using determination of the genes number, chromosome and continued using enhancement of head length one after another within every runs. Simultaneously, by consideration of performance as criteria the testing and training process, were monitored.
IV. Selection of the linking function
V. Determination of genetic operators as:
   a) Mutation

This operator has the highest efficient operator within the length of chromosome with intrinsic modification power. Mutation is able to change the terminal or function each other in the head and convert the terminal to each other in the tail.

b) Inversion

This operator is activated within the head of chromosomes and able to reverse a fragment with the length of 1–3.

c) Transposition

This operator including three types as insertion sequence (IS) transposition, (i.e., responsible for the transportation of a fragment or terminal from one position to its own head or other genes), root insertion sequence (RIS) transposition (i.e., responsible for the transportation of a fragment with its own function from first position to the changes root), gene transposition (i.e., responsible to transport the operators of all genes to the beginning of the chromosomes [61,64].

Table 3 List of function sets.

Function set	Functions
F1	$+, -, \times, \tilde{A}\cdot, Exp, Ln, x^2, 1/x, \sin andcos$
F2	$+, -, \times, \tilde{A}\cdot, Exp, Ln, x^2 and sin$
F3	$+, \times, \tilde{A}\cdot, Log, \sin andcos$
F4	$+, \tilde{A}\cdot, \sin andcos$
F5	$+, -, Exp, Ln, x^2 and tan$
F6	$+, -, \times, \tilde{A}\cdot, Exp, Ln, x^2, 1/x, x^{(1/3)} and arctan$
F7	$+, \times, Exp, LOG, x^2, x^3, \sin andcos$

Table 4 shows the range of GEP parameters for proposed models in this study. GeneXproTools 5.0 software, i.e., a powerful application, was employed to model the relation between the practical parameters of electrospunnning and diameter nanofiber of Nylon 6,6. This study tried to predict the diameter nanofiber prepared via electrospunnning method using of GEP approach. Hence, the practical parameters, i.e., *C, V, R* and *D* were selected as inputs and the diameter nanofiber selected as output (Table 1). Among 102 experimentally collected sets, 71 sets were randomly selected as training set for GEP modeling and the remaining data set were employed as testing to construct the GEP models for prediction.

2.5. Genetic algorithm

Genetic algorithms are a class of numerical optimizers which are especially useful for the resolving of complex problems, both nonlinear and nonconvex [35,65,66]. Fig. 5 depicts a flowchart of the entire GA algorithm process for all controllers.

3. Results and discussion

The root-mean-square-error (RMSE), mean absolute percentage deviation (MAPD) and root relative square error (RRSE) are among these criteria. The numerical value of the squared regression (R2), which is another parameter for estimating the model's accuracy, is also used to analyze the consistency of predicted and experimental results. The following equations yield the errors and regression value:

$$\mathrm{RMSE} = \sqrt{\frac{1}{\mathrm{N}}\sum_{1}^{\mathrm{N}}\left(y_p - y_a\right)^2} \tag{4}$$

$$\mathrm{MAPE} = \frac{1}{\mathrm{N}}\sum_{1}^{\mathrm{N}}\left(\frac{\left|y_a - y_p\right|}{y_a} \times 100\right) \tag{5}$$

$$RRSE = \sqrt{\frac{\sum_i (t_i - p_i)^2}{\sum_i \left(t_i - \left(\frac{1}{n}\right)\sum_i t_i\right)^2}} \tag{6}$$

$$\mathrm{R}^2 = 1 - \frac{\sum_{\mathrm{i}=1}^{\mathrm{n}}\left(y_a - y_p\right)^2}{\sum_{\mathrm{i}=1}^{\mathrm{n}}\left(y_a - \mathrm{y}_a^2\right)^2} \tag{7}$$

Table 4 Parameters for GEP models.

Parameter	Value
Chromosomes (P_1)	30, 35 and 40
Head size (P_2)	8, 9 and 10
Genes (P_3)	3, 4 and 5
Linking function (P_4)	Multiplication ($\times$) and Addition ($+$)
Function set	F1, F2, F3, F4, F5, F6 and F7
Mutation rate	0.0026
Inversion rate	0.01
Constants per gene	10
Training sample	71
Testing sample	31
Fitness function	RRSE

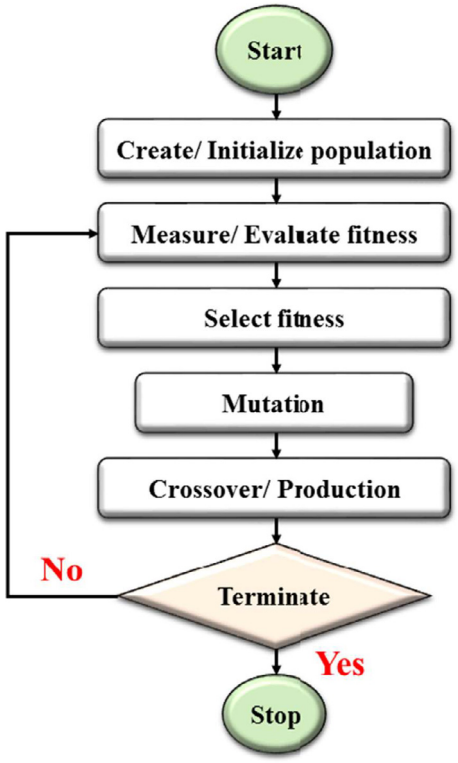

Fig. 5 A typical GA flowchart.

The y_a is the actual value, y_p is the predicted value and N is the total number of datasets. Higher R^2 and lower RMSE, RRSE, and MAPE values suggest a more precise approximation, which is the purpose of the evaluation. Summary of the statistics of the six GEP models is given in Table 5.

As concerned with the statistical results in Table 5, the seven GEP models in training and testing phases yield R^2 that is greater than 0.8625. The largest R^2 was obtained by the Gep-7 model as 0.9149 and 0.8921, respectively for the training and testing phases of the model. It is observed that the correlations between training and testing in most of the GEP models are not significantly different from each other.

For each of the six GEP-based models, R^2 is illustrated in Fig. 6(a). The R2 in the highest state (0.9149) is associated with the GEP-7 model, while the R^2 in the minimum state is 0.8625 for the GEP-6 model, as seen in this figure for a training mode. In testing mode as shown in Fig. 6, the highest value of R^2 (0.8921) is related to the models GEP-7, while the lowest one (0.6173) was reported for the GEP-6 model. In general, all of the seven GEP models are accurate in predicting diameter of Nylon 6,6 nanofiber, however, model GEP-7is preferable to another model. In the same Fig. 6(b) for training mode of the RMSE in maximum state 0.0784 is the GEP-2 model and the minimum state is 0.0572 is related to the models GEP-7, it's the lowest of RMSE and in the testing mode, the maximum state 0.1429 GEP-2 model and the minimum state is 0.1118 GEP-7 model. Therefore, as shown in Fig. 6(c) the RRSE in the maximum state is 0.3712 for GEP-6 and minimum state is 0.2921 for GEP-7 model for training mode and maximum state is 0.6296 for GEP-6 and minimum state is 0.3984 for GEP-7 model for the testing mode.

Another major step is to choose the optimum setting parameters (i.e. number of chromosomes; gene head size, number of gene and linking function) for the best GEP model.

For this purpose, first, for GEP-7 change the number of chromosomes in two mode of linking function: multiplication and addition.

As seen in Table 6 and Fig. 6, the best of number of chromosome is 30 that obtain higher R^2 and lower RMSE and RRSE with linking function of addition.

For G-4 change the head size in two mode of linking function: multiplication and addition to obtain optimum head size in this study.

According to Table 7 and Fig. 7 above, the best structure of the GEP model is a G-4 model with head size 4.

It is concluded from tables and figures above that the best model in this study is M-8 with number of chromosomes 30, head size 10 and number of genes 4 with addition as Linking function.

The formulas extracted from the M-8 to predict the diameter of Nylon 6,6 nanofiber have been presented in Eq. (8). Expression tree (ET) of the M-8 model is also provided in Fig. 8. (you can download this function from https://github.com/users/Malih9068/projects/1#card-57817375)

$$\begin{aligned} Diameter = {} & sin(sin(sin(sin(exp(4.5))))) \\ & + sin\left(sin\left(sin\left(sin\left(cos\left(cos\left(D^3\right) \times V\right)\right)\right)\right)\right) \\ & + \left(cos(cos(cos(0.4) + 2C + D))^3 \times (C \times V)^3\right) \\ & + \left(\left(cos(-1.1) + C^3 + (V \times R) + (-1.1 \times R)\right)^3 \times \left(C^3 \times C\right)\right) \end{aligned} \tag{8}$$

By consideration of the amount of Nylon 6,6 nanofiber diameter by electrospunning parameter with four factors, namely the polymer concentration (% wt/v), the applied voltage (kV), the working distance (cm), and the rate of injection

Table 5 The statistical performances of the GEP models in error and R^2.

No.	P_1	P_2	P_3	P_4	Function set	Training			Testing		
						R^2	RMSE	RRSE	R^2	RMSE	RRSE
Gep-1	30	8	3	+	F1	0.9061	0.0603	0.3080	0.6849	0.1281	0.5816
Gep-2	30	8	3	+	F2	0.8973	0.0784	0.3204	0.7878	0.1429	0.5188
Gep-3	35	9	4	+	F3	0.8945	0.0636	0.3248	0.6490	0.1384	0.6279
Gep-4	40	10	3	×	F4	0.8885	0.0696	0.3554	0.8648	0.1235	0.5602
Gep-5	30	10	5	+	F5	0.8960	0.0632	0.3226	0.6681	0.1340	0.6084
Gep-6	40	8	4	+	F6	0.8625	0.0727	0.3712	0.6173	0.1387	0.6296
Gep-7	35	10	4	×	F7	0.9149	0.0572	0.2921	0.8921	0.1118	0.3984

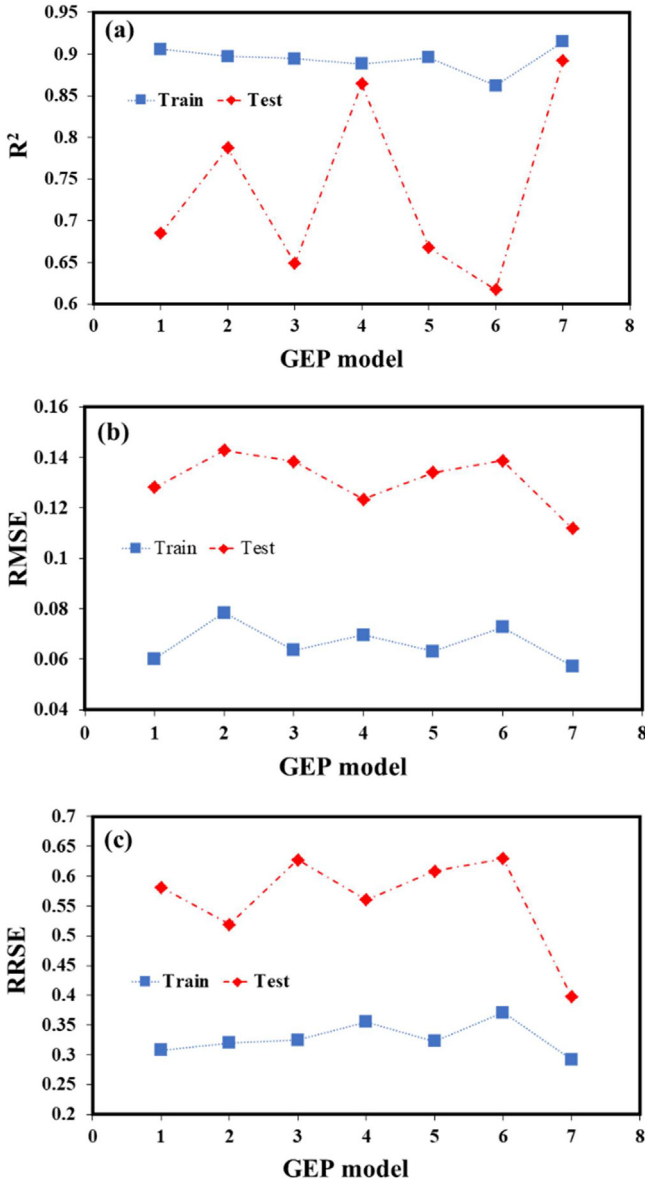

Fig. 6 The comparison of validation GEP models criteria (a) R^2, (b) RMSE and (c) RRSE values for training and testing datasets.

(mL/h), were considered as input variables of the GEP model M-8 and the average of the nanofibers diameter was chosen as the output. Table 8 can be used to check this model.

According to Table 8, GEP model is the best predict for diameter but for using this nanofiber for filter layer in the mask, diameter of nanofiber should affect the COVID-19 diameter. What's more, nanofiber should have least than 60 nm diameter tounresponsive COVID-19 in the inner layer.

In this study, using the GA model for find the minimum diameter of Nylon 6,6 model so add GEP model M-8 in the GA tools in the Matlab [67]. The GA was used with a single point crossover and roulette wheel selection. A fitness function is used to prepare each individual (i.e., the output of GEP model M-8). Optimization studies assessing the GA performance for construction design showed that the population should be small and that the rate of mutation should be low [68]. The following are the GA settings for a mixed-integer problem used in this study:

- Population size: max (min(10* number of variables, 100),40),
- Creation function: default (Constraint dependent),
- Fitness scaling: default (Rank scale),
- Selection function: default (Stochastic uniform),
- Elite count: 0.05*max (min(10* number of variables, 100),40),
- Crossover fraction: default (0.8),
- Mutation/Crossover function: default (Constraint dependent),
- Migration direction: forward (fraction: 0.2 interval: 20 by default),
- Constrain parameters: default (Augmented Lagrangian),
- Stopping criteria: (Generations: 100* number of variables, stall generations:50.

To follow GA models, four factors were considered as input variables of the GA method in this work to study the effect of working distance and injection rate on the nanofibers diameter, namely the polymer concentration (16% wt/v), the applied voltage (26 kV), the working distance (18 cm), and the injection rate (0.2 mL/h), and the average of the nanofibers diameter was 55.8 nm. High-directional nanofibers are formed when the voltage is 26 kV, and the fiber surface is smooth with a spider-like structure. The spider-like network connects the main fibers, and its formation is mainly attributable to hydrogen bonding. The average diameter of the fibres increased as the applied voltage increased. Nanofiber diameters are smaller when the concentration and voltage are higher. When the distance between the nanofibers is reduced and the injection velocity is increased, the nanofiber diameter gets bigger. Elec-

Table 6 Change in number of chromosomes for GEP-7 model upon criteria R^2, RMSE and RRSE in multiplication and addition mode.

No.	P1	P2	P3	P4	Training			Testing		
					R^2	RMSE	RRSE	R^2	RMSE	RRSE
G-1	30	10	4	×	0.9009	0.0617	0.3151	0.7166	0.1443	0.5547
G-2 (Gep-7)	35	10	4	×	0.9149	0.0572	0.2921	0.8921	0.1118	0.3984
G-3	40	10	4	×	0.9100	0.0590	0.3012	0.6662	0.1351	0.6133
G-4	30	10	4	+	0.9219	0.0447	0.2794	0.8967	0.1116	0.3597
G-5	35	10	4	+	0.8608	0.0733	0.3743	0.6657	0.1320	0.5993
G-6	40	10	4	+	0.9163	0.0569	0.2904	0.7921	0.1303	0.5913

Table 7 Change in head size for G-4 model upon criteria R^2, RMSE and RRSE in multiplication and addition mode.

No.	P1	P2	P3	P4	Training			Testing		
					R^2	RMSE	RRSE	R^2	RMSE	RRSE
M-1	30	8	3	+	0.8878	0.0656	0.3352	0.6718	0.1350	0.6128
M-2	30	8	4	+	0.9029	0.0610	0.3116	0.6985	0.1254	0.5692
M-3	30	8	5	+	0.9056	0.0617	0.3071	0.7516	0.1211	0.5496
M-4	30	9	3	+	0.8935	0.0641	0.3274	0.7405	0.1206	0.5475
M-5	30	9	4	+	0.8907	0.0647	0.3305	0.6808	0.1318	0.5981
M-6	30	9	5	+	0.8919	0.0644	0.3288	0.6680	0.1313	0.5958
M-7	30	10	3	+	0.8928	0.0641	0.3273	0.6829	0.1293	0.5868
M-8(G-4)	30	10	4	+	0.9219	0.0447	0.2794	0.8967	0.1116	0.3597
M-9	30	10	5	+	0.9028	0.0610	0.3117	0.7450	0.1180	0.5358

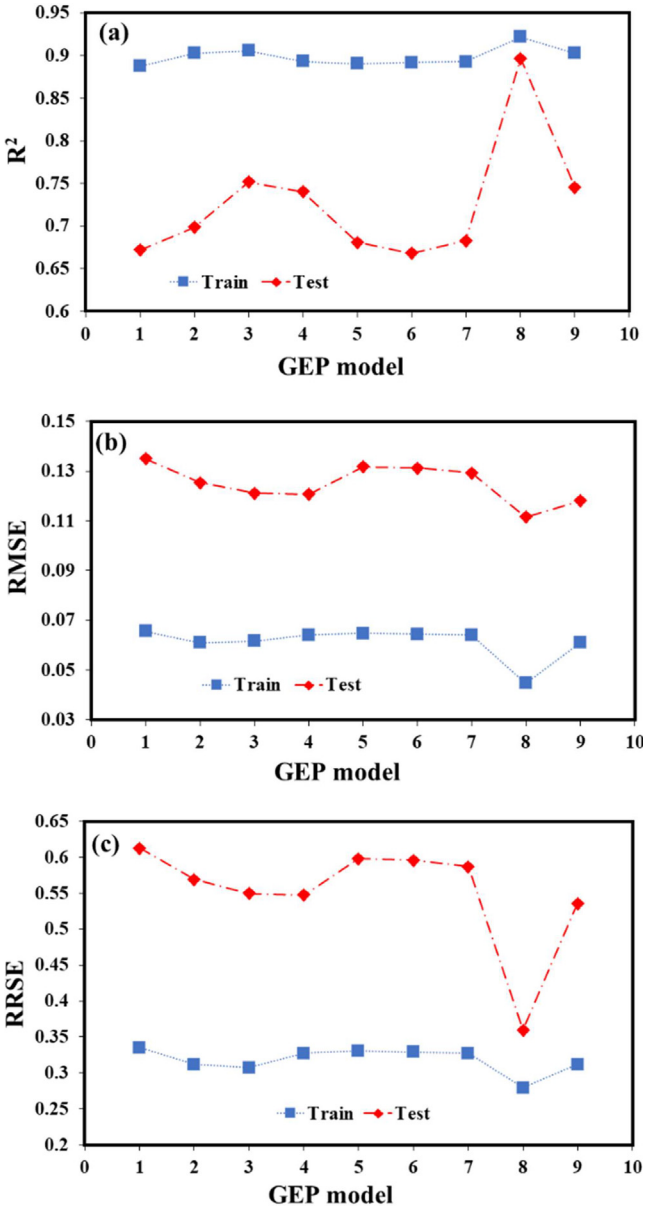

Fig. 7 Change in head size for G-4 model upon criteria R2, RMSE and RRSE in multiplication and addition mode.

trospun Nylon-6,6 nanofibers may have antiviral activity due to their porous structure and electrostatic interactions. Nanostructured surfaces with nanopillar-like architecture, such as those found on dragonfly (cicada) wings or gecko skins, are being studied in depth in order to produce biomimetic nanostructured antimicrobial surfaces [69]. Traditional antimicrobial strategies may be replaced by these nano-morphologies, which do not require the use of drugs or chemicals.

According to some studies, the diameter of nanofibers and the working distance have a direct relationship [70]. This is due to a decrease in electrostatic field strength, which causes the fibers to stretch less [71,72]. A typical SEM image of the prepared samples is shown in Fig. 9. The histogram of the size distribution of nanofibers with an average diameter of 100 ± 25 nm was determined. The results of scanning electron microscopy (SEM) revealed a fibrous structure similar to a spider web and no noticeable bead in the samples. Electrospinning spider webs can increase the specific surface area of a membrane and improve surface activity, as well as increase the porous structure, promote electrolyte transport, reduce impedance, and improve electrochemical properties. ASTM standards were used to test the particulate filtration efficiency of the newly developed nanofibrous membrane mask, which was found to be 98.6%.

The porosity of prepared membrane can be obtained using following Eq. (10):

$$Porosity(\%) = (w_w - w_d)\rho^{-1}V^{-1} \times 100\% \quad (10)$$

In this Eq, w_d and w_w are weight of membrane in dry and wet, respectivety Also, ρ shows density of formic acid, and V is geometric volume of membrane. According to results obtained from Eq. (10), the porosity of electrospun nylon-6,6 nanofibers was 84.3%.

As a result of these findings, researchers concluded that the nanofibrous membrane can be used as a powerful airborne filter against coronaviruses without compromising its filtering efficiency.

4. Conclusion

In this experiment, nylon-6,6 nanofibers as protector against coronavirus is successfully prepared by electrospinning technology. The prediction andoptimization for the diameter of electrospun Nylon-6,6 nanofiber as a function of rate, voltage, distance, and concentration using artificial intelligence such as

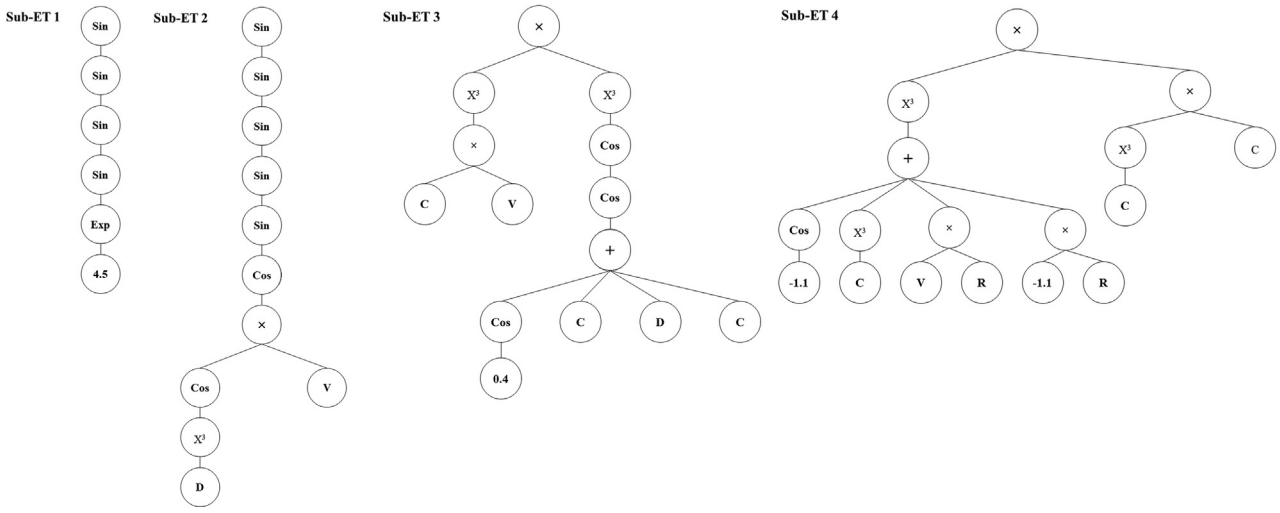

Fig. 8 Expression tree (ET) of the M-8 model.

Table 8 Effect of concentration, voltage, distance and rate on observed and predicted diameter.

Concentration (C) (% wt/v)	Voltage (V) kV)	Distance (D) cm)	Rate (R) mL/h)	Observed diameter nm)	Predicted diameter (nm)	Error
16.000	26.000	13.000	1.500	70.400	70.397	0.003
16.000	26.000	8.000	0.600	78.701	78.688	0.013

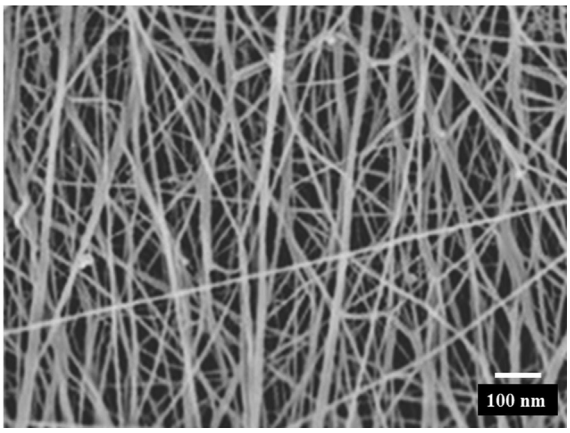

Fig. 9 SEM image of nylon-6,6 nanofibers for facemasks.

GEP and GAs. At electospinning voltage of 26 kV, nanofibers with are formed, and the fiber surface is smooth with a spider-like structure. The electrospinning method produces nylon-6,6 nanofiber webs with a high specific surface area and a porosity of up to 80%. It could be used as active layers in COVID-19 face masks.

Declaration of Competing Interest

The authors declare that they have no known competing financial interests or personal relationships that could have appeared to influence the work reported in this paper.

References

[1] H.-L. Wu, J. Huang, C.J. Zhang, Z. He, W.-K. Ming, EClin. Med. 21 (2020) 100329.
[2] D.K. Chu, E.A. Akl, S. Duda, K. Solo, S. Yaacoub, H.J. Schünemann, A. El-harakeh, A. Bognanni, T. Lotfi, M. Loeb, Lancet 395 (2020) 1973–1987.
[3] Leung, W. W. F., & Sun, Q. (2020). Charged PVDF multilayer nanofiber filter in filtering simulated airborne novel coronavirus (COVID-19) using ambient nano-aerosols. *Separation and purification technology*, *245*, 116887.
[4] Roghani, A. (2021). The Influence of COVID-19 Vaccination on Daily Cases, Hospitalization, and Death Rate in Tennessee, United States: Case Study. *Jmirx med*, *2*(3), e29324.
[5] Lin, S., Lee, C. K., Lee, S. Y., Kao, C. L., Lin, C. W., Wang, A. B., ... & Huang, L. S. (2005). Surface ultrastructure of SARS coronavirus revealed by atomic force microscopy. *Cellular microbiology*, *7*(12), 1763-1770.
[6] Goldsmith, C. S., Tatti, K. M., Ksiazek, T. G., Rollin, P. E., Comer, J. A., Lee, W. W., ... & Zaki, S. R. (2004). Ultrastructural characterization of SARS coronavirus. *Emerging infectious diseases*, *10*(2), 320.
[7] Harris, A., Cardone, G., Winkler, D. C., Heymann, J. B., Brecher, M., White, J. M., & Steven, A. C. (2006). Influenza virus pleiomorphy characterized by cryoelectron tomography. *Proceedings of the National Academy of Sciences*, *103*(50), 19123-19127.
[8] Sugita, Y., Noda, T., Sagara, H., & Kawaoka, Y. (2011). Ultracentrifugation deforms unfixed influenza A virions. *The Journal of general virology*, *92*(Pt 11), 2485.
[9] S.A. Grinshpun, M. Yermakov, J. Aerosol Sci. (2021) 105847.
[10] S.-A. Tabatabaeizadeh, Eur. J. Med. Res. 26 (2021) 1–6.

[11] K. McMahon, D. Jeanmonod, R. Check, L. Rivard, V. Balakrishnan, B. Kelly, J. Pester, R. Jeanmonod, Am. J. Emerg. Med. 48 (2021) 273–275.
[12] K. Zhang, Q. Huo, Y.-Y. Zhou, H.-H. Wang, G.-P. Li, Y.-W. Wang, Y.-Y. Wang, ACS Appl. Mater. Interfaces 11 (2019) 17368–17374.
[13] L. Séon, P. Lavalle, P. Schaaf, F. Boulmedais, Langmuir 31 (2015) 12856–12872.
[14] A. Sharma, S.R. Kumar, V. Katiyar, P. Gopinath, Nano-Struct. Nano-Objects 26 (2021) 100708.
[15] M. Karmacharya, S. Kumar, O. Gulenko, Y.-K. Cho, ACS Appl. Biol. Mater. 4 (2021) 3891–3908.
[16] Q. Xue, X. Kan, Z. Pan, Z. Li, W. Pan, F. Zhou, X. Duan, Biosens. Bioelectron. 186 (2021) 113286.
[17] J. Langmaier, Z. Samec, Electrochem. Commun. 9 (2007) 2633–2638.
[18] Z. Wang, T.C. Wang, Zhejiang Tian Cheng Environ. Technology Co., Ltd (2020).
[19] P. Dong, T. Zhang, H. Xiang, X. Xu, Y. Lv, Y. Wang, C. Lu, J. Mater. Chem. B 9 (2021) 958–968.
[20] Z. Wang, T. Zhang, L. Pi, H. Xiang, P. Dong, C. Lu, T. Jin, Colloids Surf., B 198 (2021) 111480.
[21] J. Xue, T. Wu, Y. Dai, Y. Xia, Chem. Rev. 119 (2019) 5298–5415.
[22] C. Mit-uppatham, M. Nithitanakul, P. Supaphol, Macromol. Chem. Phys. 205 (2004) 2327–2338.
[23] Lala, N. L., Ramaseshan, R., Bojun, L., Sundarrajan, S., Barhate, R. S., Ying-jun, L., & Ramakrishna, S. (2007). Fabrication of nanofibers with antimicrobial functionality used as filters: protection against bacterial contaminants. *Biotechnology and bioengineering*, *97*(6), 1357-1365.
[24] Piperno, S., Passacantando, M., Santucci, S., Lozzi, L., & La Rosa, S. (2007). WO 3 nanofibers for gas sensing applications. *Journal of applied physics*, *101*(12), 124504.
[25] Song, M., Guo, D., Pan, C., Jiang, H., Chen, C., Zhang, R., ... & Wang, X. (2008). The application of poly (N-isopropylacrylamide)-co-polystyrene nanofibers as an additive agent to facilitate the cellular uptake of an anticancer drug. *Nanotechnology*, *19*(16), 165102.
[26] Sargazi, G., Afzali, D., Mostafavi, A., & Kazemian, H. (2020). A novel composite derived from a metal organic framework immobilized within electrospun nanofibrous polymers: An efficient methane adsorbent. *Applied Organometallic Chemistry*, *34*(3), e5448.
[27] S. Zhang, W.S. Shim, J. J. M. Kim and Design 30 (2009) 3659–3666.
[28] X.F. Wu, Y.A. Dzenis, Size effect in polymer nanofibers under tension, Journal of Applied Physics 102 (4) (2007) 044306.
[29] J.-H. He, Y.-Q. Wan, L.J.C. Xu, Solit. Fractals 33 (2007) 26–37.
[30] C. Zhao, S. Zhong, X. Zhang, Q. Zhong, K. Shi, Int. J. Robust Nonlinear Control 30 (2020) 4022–4042.
[31] L. Wang, T. Yang, B. Wang, Q. Lin, S. Zhu, C. Li, Y. Ma, J. Tang, J. Xing, X. Li, Sci. Adv. 6 (2020) eaaz1622.
[32] Sukigara, S., Gandhi, M., Ayutsede, J., Micklus, M., & Ko, F. (2003). Regeneration of Bombyx mori silk by electrospinning—part 1: processing parameters and geometric properties. *Polymer*, *44*(19), 5721-5727.
[33] Naderi, N., Agend, F., Faridi-Majidi, R., Sharifi-Sanjani, N., & Madani, M. (2008). Prediction of nanofiber diameter and optimization of electrospinning process via response surface methodology. *Journal of nanoscience and nanotechnology*, *8*(5), 2509-2515.
[34] Giri Dev, V. R., Venugopal, J. R., Senthilkumar, M., Gupta, D., & Ramakrishna, S. (2009). Prediction of water retention capacity of hydrolysed electrospun polyacrylonitrile fibers using statistical model and artificial neural network. *Journal of Applied Polymer Science*, *113*(5), 3397-3404.
[35] Zeraati, M., & Khayati, G. R. (2018). Optimization of micro hardness of nanostructure Cu-Cr-Zr alloys prepared by the mechanical alloying using artificial neural networks and genetic algorithm. *Journal of Ultrafine Grained and Nanostructured Materials*, *51*(2), 183-192.
[36] Faridi-Majidi, R., Ziyadi, H., Naderi, N., & Amani, A. (2012). Use of artificial neural networks to determine parameters controlling the nanofibers diameter in electrospinning of nylon-6, 6. *Journal of applied polymer science*, *124*(2), 1589-1597.
[37] W.W.-F. Leung, Q. Sun, Sep. Purif. Technol. 245 (2020) 116887.
[38] A.H. Gandomi, A.H. Alavi, M.R. Mirzahosseini, F.M. Nejad, J. Mater. Civ. Eng. 23 (2011) 248–263.
[39] C. Ferreira, Gene expression programming: mathematical modeling by an artificial intelligence, Springer, 2006.
[40] D. Nurwaha, X. Wang, Global J. Technol. Optim. 10 (2019) 237.
[41] S.N. Wen, J. Shieh, Mater. Trans. 55 (2014) 1800–1805.
[42] P. Singh, S.K. Srivastava, M. Yameen, B. Sivaiah, V. Prajapati, P. Prathap, S. Laxmi, B. Singh, C. Rauthan, P. Singh, J. Mater. Sci. 50 (2015) 6631–6641.
[43] D.T. Cao, L.T.Q. Ngan, T.V. Viet, C.T. Anh, Int. J. Nanotechnol. 10 (2013) 343–350.
[44] Kalantari, S. S., & Taleizadeh, A. A. (2020). Mathematical modelling for determining the replenishment policy for deteriorating items in an EPQ model with multiple shipments. *International Journal of Systems Science: Operations & Logistics*, *7*(2), 164-171.
[45] A.-H. Chiou, T.-C. Chien, C.-K. Su, J.-F. Lin, C.-Y. Hsu, Curr. Appl Phys. 13 (2013) 717–724.
[46] Y. Benjamini, Am. Stat. 42 (1988) 257–262.
[47] D. Wang, Y. Ju, H. Shen, L. Xu, Constr. Build. Mater. 197 (2019) 464–473.
[48] J. Luo, M. Li, X. Liu, W. Tian, S. Zhong, K. Shi, J. Franklin Inst. 357 (2020) 39–58.
[49] B. Tiryaki, Eng. Geol. 99 (2008) 51–60.
[50] A.R. Sayadi, M.R. Khalesi, M.K. Borji, Miner. Eng. 55 (2014) 96–102.
[51] A.R. Sayadi, A. Lashgari, J.J. Paraszczak, Tunn. Undergr. Space Technol. 27 (2012) 133–141.
[52] H.F. Kaiser, Psychometrika 39 (1974) 31–36.
[53] R.S. Faradonbeh, M. Monjezi, Eng. Comput. 33 (2017) 835–851.
[54] Fan, P., Deng, R., Qiu, J., Zhao, Z., & Wu, S. (2021). Well logging curve reconstruction based on kernel ridge regression. *Arabian Journal of Geosciences*, *14*(16), 1-10.
[55] Kayadelen, C. (2011). Soil liquefaction modeling by genetic expression programming and neuro-fuzzy. *Expert Systems with Applications*, *38*(4), 4080-4087.
[56] Bathaei, B. (2016). Change is of the essence, regenerating of brown fields (landscape revitalization of Tehran's brick kilns). In *Proceedings of the 2nd International Conference on Architecture, Structure and Civil Engineering (ICASCE'16)*.
[57] Z. Li, B.Y. Bejarbaneh, P.G. Asteris, M. Koopialipoor, D.J. Armaghani, M. Tahir, Soft. Comput. (2021) 1–19.
[58] Eskandanı, O. H. (2021). Redevelopment of Brownfields, an Approach toward Sustainable Local Development. *Turkish Journal of Computer and Mathematics Education (TURCOMAT)*, *12*(13), 4808-4815.
[59] Sarıdemir, M. (2014). Effect of specimen size and shape on compressive strength of concrete containing fly ash: Application of genetic programming for design. *Materials & Design (1980-2015)*, *56*, 297-304.
[60] A. Keshavarz, H. Tofighi, Sci. Iran. 27 (2020) 2704–2718.
[61] S. Bhowmik, A. Paul, R. Panua, S.K. Ghosh, D. Debroy, Fuel 235 (2019) 317–325.
[62] M. Khosravi, M. Zeraati, J. Particle Sci. Technol. 5 (2020) 145–159.

[63] M.M. Saber, S.B. Mirtajani, K. Karimzadeh, J. Drug Delivery Sci. Technol. 47 (2018) 375–379.
[64] L.-W. Liu, Y.-M. Wang, Water 11 (2019) 1479.
[65] C.D. Chapman, Massachusetts Inst. Technol. (1994).
[66] N.J. Vickers, Curr. Biol. 27 (2017) R713–R715.
[67] Chipperfield, A. J., & Fleming, P. J. (1995). The MATLAB genetic algorithm toolbox.
[68] S.N. Al-Saadi, K.S. Al-Jabri, J. Build. Eng. 32 (2020) 101712.
[69] S. Basak, G. Packirisamy, Nano-Struct. Nano-Objects 24 (2020) 100620.
[70] M. Costolo, J. Lennhoff, R. Pawle, E. Rietman, A. Stevens, Nanotechnology 19 (2007) 035707.
[71] C. Rambo, J. Cao, O. Rusina, H. Sieber, Carbon 43 (2005) 1174–1183.
[72] Z. Chen, H. Zhang, X. He, G. Fan, X. Li, Z. He, G. Wang, L. Zhang, BioResources (2021) 16.